

Synchronization of internal and external degrees of freedom of atoms in a standing laser wave

V.Yu. Argonov and S.V. Prants

*Laboratory of Nonlinear Dynamical Systems,
V.I. Il'ichev Pacific Oceanological Institute of the Russian Academy of Sciences,
690041 Vladivostok, Russia*

(Dated: October 23, 2018)

We consider dissipative dynamics of atoms in a strong standing laser wave and find a nonlinear dynamical effect of synchronization between center-of-mass motion and internal Rabi oscillations. The synchronization manifests itself in the phase space as limit cycles which may have different periods and riddled basins of attraction. The effect can be detected in the fluorescence spectra of atoms as equidistant sideband frequencies with the space between adjacent peaks to be inversely proportional to the value of the period of the respective limit cycle. With increasing the intensity of the laser field, we observe numerically cascades of bifurcations that eventually end up in settling a strange chaotic attractor. A broadband noise is shown to destroy a fine structure of the bifurcation scenario, but prominent features of period-1 and period-3 limit cycles survive under a weak noise. The character of the atomic motion is analyzed with the help of the friction force whose zeroes are attractor or repeller points in the velocity space. We find ranges of the laser parameters where the atomic motion resembles a random but deterministic walking of atoms erratically jumping between different wells of the optical potential. Such a random walking is shown to be fractal in the sense that the measured characteristic of the motion, time of exit of atoms from a given space of the standing wave, is a complicated function that has a self-similar structure with singularities on a Cantor set of values of one of the control parameters.

PACS numbers: 42.50.Vk, 05.45.Mt, 05.45.Xt

I. INTRODUCTION

Light exerts mechanical forces on neutral atoms whose origin can be explained as in the particle as in the wave pictures of the particle-wave duality. In the first one, light is a collection of photons carrying energy, angular momentum, and momentum. When interacting with light, atoms change not only their internal electronic states but also their external translational states, the process known as a photon recoil. If one considers light as a wave, the mechanical force is produced by the interaction between inhomogeneous electromagnetic wave and the atomic dipole moment.

In this paper we consider atoms confined in a cavity or in a standing wave made up of two counter-propagating laser waves. There is a vast literature on the various aspects of the topic of mechanical action of light on atoms (see, for example, some reviews and books [1, 2, 3, 4, 5]). In the simplest case of a two-level atom interacting with a single mode of an one-dimensional standing wave in a cavity, there are, at least, three strongly coupled subsystems: internal and external atomic degrees of freedom and field degrees of freedom. Recently, it has been shown theoretically and numerically that Hamiltonian dynamics of a single atom in a standing light wave demonstrates a variety of new dynamical effects such as correlations between Rabi oscillations and atomic translational motion [6, 7], the Doppler-Rabi resonance [7, 8], Hamiltonian chaos [9, 10], Lévy flights [7, 11, 12], and atomic dynamical fractals [7, 12, 13]. The semiclassical and quantum theory of these effects has been developed in the cited

papers.

In the present paper we study dissipative dynamics of two-level atoms in a standing wave pumped by a laser and report on a nonlinear dynamical effect of synchronization between internal and external atomic degrees of freedom. Light-induced forces cause an atom either to be trapped in a well of the optical potential or to fly through the standing wave. The mechanical atomic oscillator forces the Rabi one to oscillate with the same rhythm. Synchronization occurs after a transition time and manifests itself in the phase space as limit cycles which may have different periods depending on the detuning δ between the atomic transition, ω_a , and standing-wave frequencies, ω_f , and on the average number of photons in the wave n . Synchronization and the period of the respective limit cycle can be detected by measuring fluorescence spectra of atoms. Synchronized ballistic motion with a period- m limit cycle should generate sidebands with the frequencies, $\omega_f \pm jk_f v_s/m$ ($j = 1, 2, \dots$) in the respective spectra (where v_s is a quasistationary atomic velocity), whereas trapped atoms, oscillating under a period- m limit cycle, generate sidebands $\omega_f \pm j\Omega_\xi/m$, where Ω_ξ is the respective frequency of nonlinear synchronized oscillations. Asynchronous chaotic motion generates a broaden spectrum.

This work is organized as follows: in Sec. II the model of an atom interacting with a standing wave in a driven cavity is introduced, and semiclassical equations of motion including spontaneous relaxation, cavity damping, and pumping are derived. In the strong-field limit and under a resonance of a laser with the standing wave, the equations are reduced to a five-dimensional dissipa-

tive nonlinear system with coupled mechanical and Bloch variables. In Sec. III we discuss briefly two simple regimes of atomic motion: shallow oscillations of an atom trapped in the optical potential and ballistic motion under an influence of the light-induced friction force. The friction force is analytically calculated for thermal atoms with a large detuning δ . In Sec. IV we report on synchronization of the atomic Rabi oscillations with the momentum oscillations, give respective approximated analytic solutions for period-1 limit cycles, show that basins of attraction of different limit cycles are riddled, and compute spectra of atomic fluorescence. In Sec. V we demonstrate a rich scenario of bifurcations in dependence on the average number of photons in the standing wave. The scenario contains coexisting limit cycles of different periods, period doubling, and cascades of different bifurcations on the road to a strange chaotic attractor. Sec. VI contains numerical results demonstrating atomic dynamical fractals in the regime of random walking of an atom in a standing wave and a comparison between dissipative and Hamiltonian fractals.

II. EQUATIONS OF MOTION

Let us consider a two-level atom with the electronic transition frequency ω_a and mass m_a in a 1D-cavity which sustains a single cosine-like standing-wave mode along the axis r with the wave number k_f and the frequency ω_f . The cavity mode is supposed to be pumped by a classical laser field with the amplitude ε , phase φ , and frequency ω_l . The total Hamiltonian

$$\hat{H} = \hat{H}_0 + \hat{H}_l \quad (1)$$

consists of the standard cavity QED Hamiltonian

$$\hat{H}_0 = \frac{\hat{p}^2}{2m_a} + \frac{1}{2}\hbar\omega_a\hat{\sigma}_z + \hbar\omega_f\left(\hat{a}^\dagger\hat{a} + \frac{1}{2}\right) - \hbar\Omega_0\cos(k_f\hat{r})(\hat{a}^\dagger\hat{\sigma}_- + \hat{a}\hat{\sigma}_+) \quad (2)$$

and the laser-mode interaction Hamiltonian

$$\hat{H}_l = \hbar\varepsilon\hat{a}\exp i(\omega_l t - \varphi) + \text{H. c.} \quad (3)$$

The atom may emit and absorb photons from the cavity mode. Both the processes change internal atomic and field states. The external or translational atomic states are changed as well because of a photon recoil. The laser field supplies an energy to overcome atomic and mode dissipation. All the processes are presented in the Hamiltonians. The operators \hat{r} and \hat{p} with the commutation rule $[\hat{r}, \hat{p}] = i\hbar$ describe atomic position and momentum, respectively. The Pauli atomic operators $\hat{\sigma}_\pm \equiv \frac{1}{2}(\hat{\sigma}_x \pm i\hat{\sigma}_y)$ and $\hat{\sigma}_z$ with the commutation rules $[\hat{\sigma}_\pm, \hat{\sigma}_z] = \mp 2\hat{\sigma}_\pm$, $[\hat{\sigma}_+, \hat{\sigma}_-] = \hat{\sigma}_z$ describe electronic atomic transitions. The boson operators \hat{a} and \hat{a}^\dagger with the commutator $[\hat{a}, \hat{a}^\dagger] = 1$ describe the cavity mode.

The atom-field coupling is characterized by an amplitude of the single-photon Rabi frequency Ω_0 .

It is convenient to choose the following combinations of operators: $\hat{e} \equiv \hat{a}^\dagger \exp(-i\omega_f t) + \hat{a} \exp(i\omega_f t)$, $\hat{g} \equiv i[\hat{a}^\dagger \exp(-i\omega_f t) - \hat{a} \exp(i\omega_f t)]$, $\hat{x} \equiv \hat{\sigma}_- \exp(i\omega_f t) + \hat{\sigma}_+ \exp(-i\omega_f t)$, $\hat{y} \equiv i[\hat{\sigma}_- \exp(i\omega_f t) - \hat{\sigma}_+ \exp(-i\omega_f t)]$, $\hat{\sigma}_z$, \hat{r} , and \hat{p} , for which the respective Heisenberg equations can be derived using the Hamiltonians (2) and (3) in the frame rotating with the frequency ω_f

$$\begin{aligned} \frac{d\hat{r}}{dt} &= \frac{\hat{p}}{m}, \\ \frac{d\hat{p}}{dt} &= \frac{\hbar k_f \Omega_0}{2}(\hat{g}\hat{y} - \hat{e}\hat{x})\sin(k_f\hat{r}), \\ \frac{d\hat{e}}{dt} &= \Omega_0\hat{y}\cos(k_f\hat{r}) + 2\varepsilon\sin(\omega_f t - \omega_l t + \varphi) - 2\Gamma_f\hat{e}, \\ \frac{d\hat{g}}{dt} &= \Omega_0\hat{x}\cos(k_f\hat{r}) - 2\varepsilon\cos(\omega_f t - \omega_l t + \varphi) - 2\Gamma_f\hat{g}, \\ \frac{d\hat{x}}{dt} &= (\omega_f - \omega_a)\hat{y} + \Omega_0\hat{\sigma}_z\hat{g}\cos(k_f\hat{r}) - \frac{1}{2}\Gamma_a\hat{x}, \\ \frac{d\hat{y}}{dt} &= (\omega_a - \omega_f)\hat{x} + \Omega_0\hat{\sigma}_z\hat{e}\cos(k_f\hat{r}) - \frac{1}{2}\Gamma_a\hat{y}, \\ \frac{d\hat{\sigma}_z}{dt} &= -\Omega_0(\hat{g}\hat{x} + \hat{e}\hat{y})\cos(k_f\hat{r}) - \Gamma_a(\hat{\sigma}_z + 1), \end{aligned} \quad (4)$$

where Γ_f and Γ_a are the rate of dissipation of cavity photons and spontaneous emission rate, respectively, to be added to the respective equations phenomenologically. After averaging over an initial quantum state, which is supposed to be a product of the field, internal, and external atomic states, we get the respective c-number equations of motion. Assuming a large number of photons in the cavity mode, $n = (e^2 + g^2)/4 \gg 1$, and large values of the atomic momentum as compared with the photon momentum $\hbar k_f$, we adopt the semiclassical approximation. It results in the following normalized closed set of ODEs:

$$\begin{aligned} \dot{\xi} &= \alpha p, \\ \dot{p} &= (1/2)(gy - ex)\sin\xi, \\ \dot{e} &= y\cos\xi - 2\gamma_f e + 2E\sin(\Delta\tau + \phi), \\ \dot{g} &= x\cos\xi - 2\gamma_f g - 2E\cos(\Delta\tau + \phi), \\ \dot{x} &= \delta y + zg\cos\xi - (1/2)\gamma_a x, \\ \dot{y} &= -\delta x + ze\cos\xi - (1/2)\gamma_a y, \\ \dot{z} &= -(gx + ey)\cos\xi - \gamma_a(z + 1), \end{aligned} \quad (5)$$

where dot denotes differentiation with respect to the dimensionless time $\tau \equiv \Omega_0 t$ and $E \equiv \varepsilon/\Omega_0$. Here $\xi \equiv k_f \langle \hat{r} \rangle$, $z \equiv \langle \hat{\sigma}_z \rangle$, $p = \langle \hat{p} \rangle / \hbar k_f$, and the other variables are the expectation values of the respective operators written above. A few dimensionless frequencies define the atom-field dynamics: $\alpha \equiv \hbar k_f^2 / m_a \Omega_0$ is the photon recoil frequency, $\delta \equiv (\omega_f - \omega_a) / \Omega_0$ the detuning between the frequencies of the cavity mode and

atomic electronic transition, $\Delta \equiv (\omega_f - \omega_l)/\Omega_0$ the cavity-laser detuning, and $\gamma_{a,f}$ the relaxation rates.

In fact, Eqs. (5) are the coupled Hamilton-Maxwell-Bloch equations which take into account not only light-induced mechanical forces acting on a neutral atom but the back reaction of the atom on the cavity mode as well. In a strong field the cavity mode reaches rapidly a regime with a large saturation number of photons $n = (E/2\gamma_f)^2$. Throughout the paper we will consider the case of exact resonance between the cavity mode and the laser, $\Delta = 0$, and a specified phase $\varphi = \pi/4$. It follows the reduced set of our basic equations

$$\begin{aligned}\dot{\xi} &= \alpha p, \\ \dot{p} &= -u \sin \xi, \\ \dot{u} &= \delta v - (1/2)\gamma_a u, \\ \dot{v} &= -\delta u + 2nz \cos \xi - (1/2)\gamma_a v, \\ \dot{z} &= -2v \cos \xi - \gamma_a(z + 1),\end{aligned}\quad (6)$$

where we introduce new variables $u \equiv (ex - gy)/2 = \sqrt{n/2} (x + y)$ and $v \equiv (gx + ey)/2 = \sqrt{n/2} (y - x)$ which are proportional to the quadrature components of the atomic electric dipole moment. Namely, the system (6) will be treated throughout the paper. Eqs. (6) are written in the form convenient to the comparison with equations (3) in Ref. [7] which describe Hamiltonian self-consistent atom-field dynamics in a high-Q cavity without dissipation and a pumping field. In fact, we need no cavity in the strong field regime for which Eqs. (6) are valid. A standing wave may be created by two counter propagating laser beams in a free space. Real laser beams produce, of course, a three dimensional standing wave, and we simplify the geometry to simplify the analysis.

III. CENTER-OF-MASS MOTION IN A STANDING WAVE

A. Shallow oscillations in a well of the optical potential: steady-state solutions

An atom moves in an optical potential $\Pi = \int u \sin \xi d\xi$, whose form can be easily found in the steady state approximation when the atom is assumed to move so slowly that the Bloch variables u , v , and z have a time to take steady-state values. It is the case of rather cold trapped atoms oscillating in wells of the optical potential that is valid if the normalized Doppler shift is much smaller than the detuning and the relaxation rates, $|\alpha p| \ll |\delta|, \gamma_{a,f}$. With the time derivatives of the Bloch variables in Eqs. (6) equal to zero, it is easily to find their stationary values

$$\begin{aligned}u_s &= -\frac{2n\delta \cos \xi}{\delta^2 + 2n^2 \cos^2 \xi + \gamma_a^2/4}, \\ v_s &= -\frac{\gamma_a n \cos \xi}{\delta^2 + 2n^2 \cos^2 \xi + \gamma_a^2/4}, \\ z_s &= -\frac{1}{1 + 2n^2 \cos^2 \xi / (\delta^2 + \gamma_a^2/4)}.\end{aligned}\quad (7)$$

Substituting the solution for u_s in the second equation in (6), we obtain the gradient or dipole force acting on the atom

$$\dot{p} = \frac{n\delta \sin 2\xi}{\delta^2 + 2n^2 \cos^2 \xi + \gamma_a^2/4} \quad (8)$$

and the optical potential

$$\Pi = \frac{\delta}{n} \ln \left(\frac{\gamma_a^2}{4} + \delta^2 + 2n^2 \cos^2 \xi \right). \quad (9)$$

Well known effects follow from this solution (see, for example, [2, 4]). At exact resonance, $\delta = 0$, the optical potential is zero, and the atom moves with a constant velocity, equal to its initial value $p = p_0$. At positive values of the detuning, $\delta > 0$, atoms tend to go to nodes of standing wave ($\xi = \pi/2 + \pi m$), whereas at negative detuning, $\delta < 0$, they tend to go to antinodes ($\xi = \pi m$), where $m = 0, 1, \dots$. We recall that our standing wave is of the form $-\cos \xi$.

B. Ballistic motion and the friction force

When an atom moves with a thermal average momentum p_s through the standing wave, the Doppler shift exceeds relaxation rates, and the approximation of slowly varying field amplitude is no valid. In the limit $|\alpha p_s| > \gamma_{a,f}$, we will seek solutions for the Bloch variables in the form

$$\begin{aligned}u &= A \cos \alpha p_s \tau + B \sin \alpha p_s \tau, \\ v &= C \cos \alpha p_s \tau + D \sin \alpha p_s \tau.\end{aligned}\quad (10)$$

Let the atom reaches after a transition time a quasistationary momentum p_s (around which its instant momentum oscillates slightly) and does not experience Rabi oscillations due to a large detuning $|\delta| \gg 1$, i. e. $z \simeq -1$. Substituting the solutions (10) into Eqs. (6), it is possible to find after some algebra an expression for the force acting on the atom $f \equiv \dot{p} = -u \sin \xi$. After time averaging it, we get a dissipative or friction force, $F \equiv -d|\bar{p}|/d\tau$, which has the form

$$F \simeq -\frac{2n\delta\gamma_a\alpha|p_s|}{(\gamma_a\delta)^2 + [(\alpha|p_s|)^2 - \delta^2 + \gamma_a^2/4]^2}. \quad (11)$$

This approximated solution gives dispersion-like dependencies on the Doppler shift $\alpha|p_s|$ and the detuning δ . At negative detunings, the friction force decelerates atoms whereas at positive detunings, it accelerates them.

In fact, the friction force F depends on $\alpha|p_s|$ and δ in a more complicated way. We integrate the basic Eqs. (6) and plot in Fig. 1 its dependence on instant values of the atomic momentum $|\bar{p}|$, averaged over a time of flight between two successive nodes of the standing wave, at $\delta > 0$ (Fig. 1a) and $\delta < 0$ (Fig. 1b). It is plotted for the values of the momentum larger than a critical momentum p_{cr} that is a minimal value of $|\bar{p}|$ under which

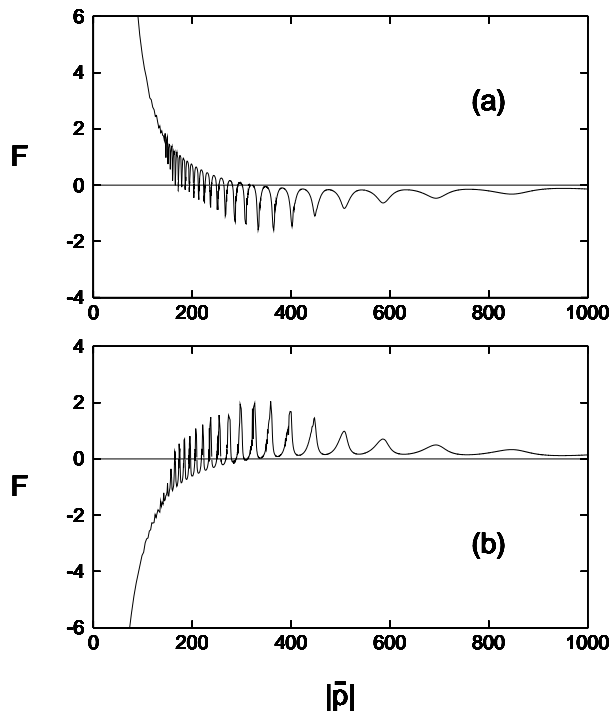


FIG. 1: Friction force F in units of $\Omega_0 \hbar k_f$ as a function of the average atomic momentum $|\bar{p}|$ in units of the photon momentum $\hbar k_f$. (a) Positive detuning $\delta = 24$ and (b) negative detuning $\delta = -24$.

a ballistic motion is possible. What happens with atoms whose momenta at some instant of time lie in a given range? At blue detunings, $\delta > 0$, atoms with $|\bar{p}| < |p_a|$ are trapped, where $|p_a|$ is a value of the average momentum which corresponds to the first zero of the function $F(|\bar{p}|)$. The parts of this function between its successive zeroes may be considered as averaged phase trajectories of atoms in the space $(|\bar{p}|, d|\bar{p}|/d\tau)$. At positive values of the friction force, atoms move with decreasing momentum, to the left on the plot. At $F < 0$, they move with increasing momentum, i.e. to the right on the plot. Thus, zeroes of the function $F(|\bar{p}|)$ with positive derivatives are attractors, whereas zeroes with negative derivatives are repellers.

As it can be seen from Fig. 1b, at red detunings, $\delta < 0$, repellers and attractors interchange their places as compared with Fig. 1a. It immediately means that the friction at $\delta < 0$ accelerates slow atoms and decelerates fast ones which in a due time reach a quasistationary momentum $|p_s|$ and oscillate slightly in the velocity space around it (Fig. 2a). If the initial momentum is sufficiently small, an atom may even change the direction of motion, but a stabilization occurs in a due time. It is the known effect of velocity grouping [14] that appears to be useful to observe fluorescence spectra for an atomic ensemble with a velocity distribution that is a more feasible task from the

experimental point of view than observing a single-atom fluorescence. Initially trapped atoms oscillate firstly in wells of the optical potential with increasing amplitudes, and then leave the wells reaching after a transition time a grouping velocity (lower trajectory in Fig. 2a).

In difference from red detunings, where velocity grouping is global, at blue detunings it is limited in the velocity space by a range of the atomic momenta $|p_a| < |\bar{p}| < |p_b|$, containing zeroes of the function $F(|\bar{p}|)$. The values of the momenta, $|p_a|$ and $|p_b|$, corresponding to the first and last zeroes, are proportional to the detuning δ and

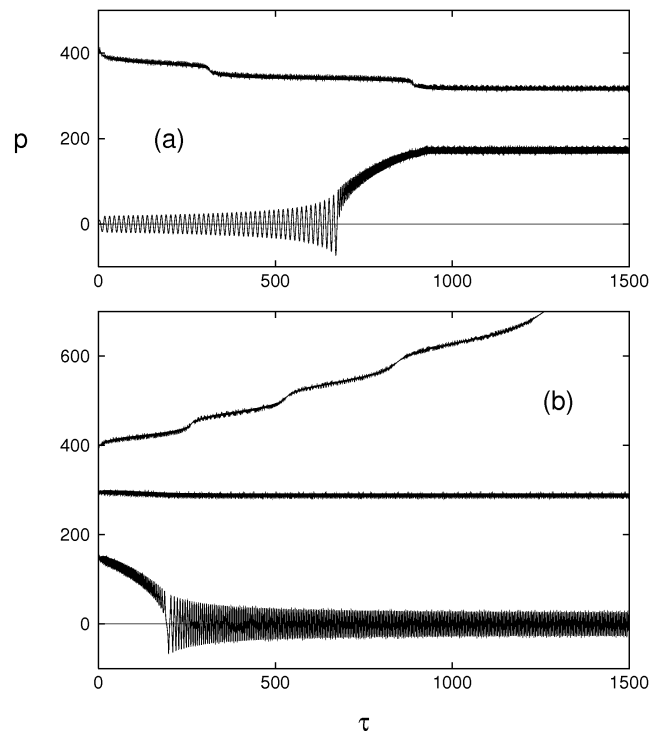


FIG. 2: Atomic momentum p as a function of time τ in units of the reciprocal of the single-photon Rabi frequency Ω_0 . (a) red detuning, $\delta < 0$: global velocity grouping for different values of the initial momentum; (b) blue detunings, $\delta > 0$: fast atoms are accelerated (upper trajectory), slow atoms are decelerated (lower trajectory), and velocity grouping occurs only for atoms in a range $|p_a| \leq |\bar{p}| \leq |p_b|$.

depend on the other control parameters in an irregular way. Thus, at $\delta > 0$, slow atoms (with $|\bar{p}| \leq |p_a| \simeq 170$ in Fig. 1a) are decelerated by the friction force and trapped in wells of the optical potential eventually (see the lower trajectory in Fig. 2b). The friction force for fast atoms ($|\bar{p}| \geq |p_b| \simeq 320$) is negative, and they are accelerated by the field (the upper trajectory in Fig. 2b). The velocity grouping at $\delta > 0$ occurs only in the range $170 \lesssim |\bar{p}| \lesssim 320$. A sample trajectory for such atoms is shown in Fig. 2b as a middle one.

IV. SYNCHRONIZATION

A. General features

Our basic Eqs. (6) describe two coupled oscillators, the external mechanical one (ξ, p) and the internal Rabi oscillator (u, v, z) whose free frequencies may differ in a few orders of magnitude in a strong field. The frequency of small oscillations of an atom in a well of the optical potential can be estimated to be $\alpha^{1/2}n^{1/4}$, whereas the free Rabi frequency, $\sqrt{\delta^2 + 4n}$, is proportional to a square root of the average number of photons n . The phenomenon we report in this section is synchronization of internal and external degrees of freedom of an atom in a standing-wave field. Synchronization is a fundamental nonlinear phenomenon to be observed for the first time by Ch. Huygens in 1665 with his famous mechanical pendulum clock [15] and described theoretically by A. Andronov and A. Witt in 1930 [16] in terms of limit cycles. In our case the effect consists in equality between the frequency of oscillations of the atomic internal energy and the frequency of variations of the atomic momentum as for trapped as for ballistic atoms. The mechanical oscillator forces the Rabi one to oscillate with the same rhythm. A standing wave with the spatial period 2π modulates with the Doppler shift αp_s momentum of an atom, moving with an average momentum p_s .

Synchronization manifests itself in the phase space as limit cycles which may have different periods. A limit cycle of period m means a periodicity occurs when the atom transverses $2m$ times the same node (being trapped in a well) or different nodes (a ballistic atom) of the standing wave. We have found limit cycles with $m=1, 2, 3, \dots, 12$. In Fig. 3a and 3b we plot projections of period-1 and period-3 limit cycles on the Bloch plane (v, u) and on the plane (ξ, z) of the internal and external variables at $\delta = 24$, $\alpha = 0.01$, $\gamma_a = 0.3$, and $p_0 = 60$. The size of a limit cycle is defined by the amplitude of the respective synchronized oscillations, its form — by the spectrum of the oscillations, and the time of circulation of a phase point over the cycle — by the period of oscillations. The larger the parameter of nonlinearity, n , the stronger the form of a limit cycle differs from the harmonic one. In Fig. 3a the dashed line is a period-1 limit cycle with $n = 3000$ and the solid one is a cycle with $n = 10000$.

Synchronization of internal and external atomic degrees of freedom is a common feature of regular motion that occurs with different initial states and in wide ranges of values of the control parameters. The only exception is the case of exact resonance, $\delta = 0$, when the optical potential vanishes and an atom flies through the wave with a constant velocity, but its internal energy oscillates with a modulated amplitude and frequency. Chaos destroys synchronization if one understands under this name a frequency locking, where two frequencies become rationally related. Synchronization of chaotic oscillations (if any) is beyond the scope of this paper.

The time of settling limit cycles depends mainly on the

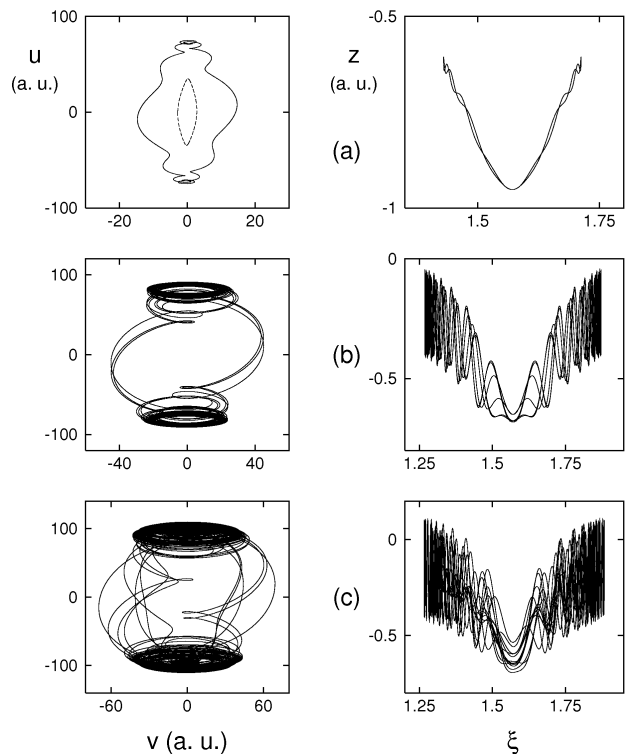


FIG. 3: Projections of the phase trajectories of a trapped atom onto two planes (u, v) and (ξ, z) at $\delta = 24$: (a) period-1 limit cycle (dashed line at $n = 3000$ and solid line at $n = 10000$), (b) period-3 limit cycle ($n = 14846$), and (c) chaotic strange attractor ($n = 24000$). The atomic position ξ is shown in units of k_f^{-1} .

action of the force f which accelerates or decelerates an atom during a transition time τ_s before it reaches a quasistationary momentum p_s . This time can be estimated for atoms with velocities p closed to p_s as follows. The force can be expanded in the Taylor series nearby the point p_s

$$\Delta f = \Delta p f'(p_s) + \dots, \quad (12)$$

where $\Delta p \equiv p_s - p$, $\Delta f \equiv f(p_s) - f(p)$, and $f' \equiv df/dp$. On the other hand, for small Δp , $\Delta f \simeq \Delta p/\tau_s$, and in the first order we get $\tau_s \simeq [f'(p_s)]^{-1}$. It follows from (11), the transition time is a reciprocal of the average number of photons n .

B. Approximated analytic solutions for period-1 cycles

Depending on the values of the control parameters and the initial momentum, atoms either are trapped in wells of the optical potential and oscillate with $p_s = 0$, or they fly through the standing wave ($p_s \neq 0$). The frequency

of synchronized motion is defined by the frequency of oscillations of p around p_s . At $\delta > 0$ and sufficiently large values of the initial momentum p_0 , atoms can move with an acceleration asymptotically going to zero (Fig. 1a and Fig. 2b, the upper trajectory).

In order to find simple analytic solutions for period-1 limit cycle in the case of ballistic motion, we put $\xi \approx \alpha p_s$ and expand the variables p , u , v , and z in Fourier series

$$u = \sum_{j=0}^{\infty} a_j^{(u)} \cos(j\alpha p_s \tau) + b_j^{(u)} \sin(j\alpha p_s \tau), \quad (13)$$

with p , v , and z being analogous Fourier series with respective coefficients. Substituting these series in the basic equations (6), we get an infinite number of recurrent relations for the coefficients. A period-1 limit cycle is described by the first terms in the Fourier series, if amplitudes of higher harmonics can be neglected. The approximated solution at large detunings can be found (truncating the hierarchy at $j = 2$) to be

$$\begin{aligned} p &\approx p_s - (\delta A_b / 2\alpha p_s) \cos 2\alpha p_s \tau, \\ u &\approx -2\delta A_b \cos \alpha p_s \tau, \\ v &\approx -\gamma_a A_b \cos \alpha p_s \tau + 2\alpha p_s A_b \sin \alpha p_s \tau, \\ z &\approx -1 + A_b(1 + \cos 2\alpha p_s \tau), \end{aligned} \quad (14)$$

where

$$A_b \equiv \frac{n}{(\delta^2 - \alpha^2 p_s^2 + n + \gamma_a^2/4)}. \quad (15)$$

The solutions (14) and (15) are valid under the condition $n \ll \delta^2 - \alpha^2 p_s^2 + \gamma_a^2/4$. Numerical simulation shows that the obtained solutions really work well under the condition of a small number of photons as compared with the squared detuning. When this condition breaks down, higher harmonics become significant, and the simple form of period-1 limit cycles is distorted.

The same procedure has been used to find analytic solutions for small oscillations of atoms in wells of the optical potential. At $\delta > 0$, the wells are situated at the nodes of the standing wave $\xi = \pi/2 + \pi m$ ($m = 0, 1, \dots$). Assuming a harmonic motion of an atom at the bottom of a well, $\xi = \pi/2 + \pi m + \xi_m \cos \omega_\xi \tau$, we find the approximated solutions for a period-1 limit cycles

$$\begin{aligned} \rho &\approx (2\delta A_w \xi_m / \omega_\xi) \sin \omega_\xi \tau, \\ u &\approx -2\delta A_w \xi_m \cos \omega_\xi \tau, \\ v &\approx -\gamma_a A_w \xi_m \cos \omega_\xi \tau + 2\omega_\xi A_w \xi_m \sin \omega_\xi \tau, \\ z &\approx -1 + A_w \xi_m^2 (1 + \cos \omega_\xi \tau), \end{aligned} \quad (16)$$

where the squared frequency of the small oscillations is

$$\omega_\xi^2 \approx -\frac{\delta^2}{2} - \frac{\gamma_a^2}{8} + \frac{1}{2} \sqrt{\left(\delta^2 + \frac{\gamma_a^2}{4}\right)^2 + 8n\alpha|\delta|} \quad (17)$$

and

$$A_w \equiv \frac{n}{\delta^2 - \omega_\xi^2 + n\xi_m^2 + \gamma_a^2/4}. \quad (18)$$

The solutions (16) – (18) are valid under the following condition: $n\xi_m^2 \ll \delta^2 - \omega_\xi^2 + \gamma_a^2/4$. Under the limits of its validity, the solutions (16) – (18) agree well with numerical simulation. Since the normalized amplitude of small oscillations, ξ_m , can be less than 1, the solutions (16) are valid up to the values of the number of photons of the order of a few thousands.

C. Riddling

For given values of the recoil frequency α and the spontaneous rate γ_a , there are many kinds of attractors when the detuning δ and the numbers of photons n are changed. For the same n and δ , different initial conditions may lead to different attractors, i. e. the system is sensitively dependent on initial conditions. It should be stressed that it may happen even under regular synchronous oscillations. We have numerically found two, three, and more coexisting stable limit cycles with the same and different periods, whose basins of attraction are riddled by each other. The basin is said to be riddled [17], if any point in the basin has in its arbitrary small vicinity points of other attractor basins.

In Fig. 4 we illustrate riddling for three coexisting limit cycles of periods 1, 2, and 3 in the plane of initial atomic momentum p_0 and population inversion z_0 . Initial conditions on 200×200 grid were integrated to find the respective limit cycles they destinate. Grid points going to the period-3 limit cycles are plotted as dark grey dots, those that go to the period-2 limit cycle — as light grey dots, and the grid points going to the period-1 limit cycle are left white. As one can see in Fig. 4, grey and white points are mixed. Since the accuracy of preparing initial conditions is finite, one cannot predict exactly which limit cycle will be destinated from a given initial point in the phase space. To confirm the riddling, we magnified a small region in Fig. 4a ($0.8 \leq z_0 \leq 1$; $60 \leq p_0 \leq 70$) and compute the basins of attraction with the same grid 200×200 . The result, shown in Fig. 4b, demonstrates that riddled basins may occur not only on chaotic and strange attractors [17] but also on stable limit cycles.

D. Spectra of fluorescence

The feasible way to detect synchronization in real experiments is to measure spectra of atomic fluorescence. Let us derive an expression for the atomic transition dipole moment in the laboratory frame of reference. Assuming the magnitude μ of the dipole d to be real, we have $d = \mu \tilde{x}$, where \tilde{x} -component of the dipole in the laboratory frame is connected to the x and y components in the frame, rotating with the frequency ω_f , by the following way:

$$\tilde{x} = x \cos \omega_f t + y \sin \omega_f t. \quad (19)$$

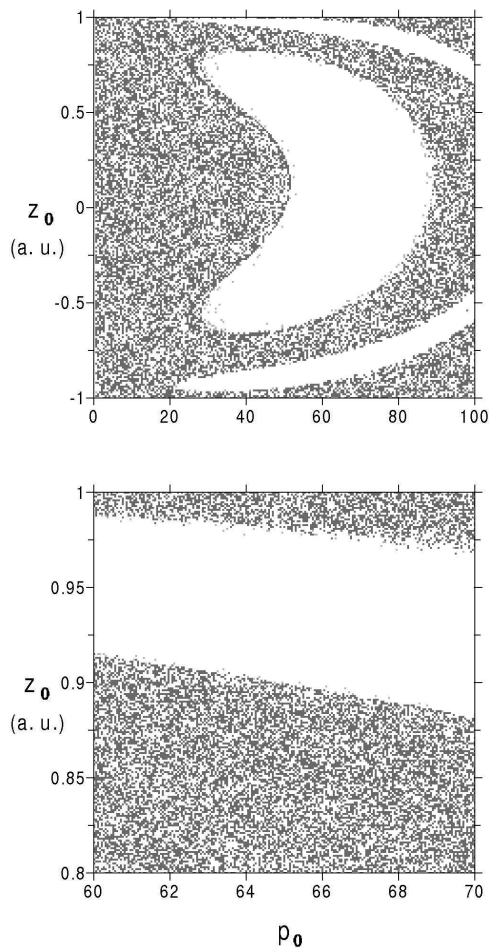


FIG. 4: Riddled basins of attraction in the plane of initial population inversion z_0 and initial momentum p_0 (in units $\hbar k_f$): \square period 1 limit cycle, \blacksquare period 2 limit cycle, \blacksquare period 3 limit cycle. (a) 200×200 grids and (b) 200×200 grids giving a magnified view of a small region in (a).

Our basic equations (6) are written in the rotating frame for the dynamical variables $u \equiv \sqrt{n/2} (x + y)$ and $v \equiv \sqrt{n/2} (y - x)$. Therefore, the expression for the atomic dipole moment in the laboratory frame is

$$d = \frac{\mu}{\sqrt{2n}} [(u - v) \cos \omega_f t - (u + v) \sin \omega_f t]. \quad (20)$$

Using the solutions (14) for a period-1 limit cycle in the ballistic mode, it is easily to find that the atomic dipole moment will oscillate with the frequencies $\omega_f \pm j k_f v_s$, where v_s is a quasistationary atomic velocity reached by atoms after a transition time, and $j = 0, 1, 2, \dots$. Dipole moments of ballistic atoms with a period- m limit cycle have the frequencies $\omega_f \pm j k_f v_s / m \equiv \omega_f \pm j \Omega_0 \alpha p_s$. Trapped atoms oscillating with a period- m limit cycle, have dipole moments oscillating with the frequencies $\omega_f \pm j \Omega_\xi / m \equiv \omega_f \pm j \Omega_0 \omega_\xi / m$, where ω_ξ is given by Eq.

(17). Fluorescence spectra both for the atoms, randomly walking in a standing wave and oscillating in wells in the regime of strange chaotic attractors, should be broadened.

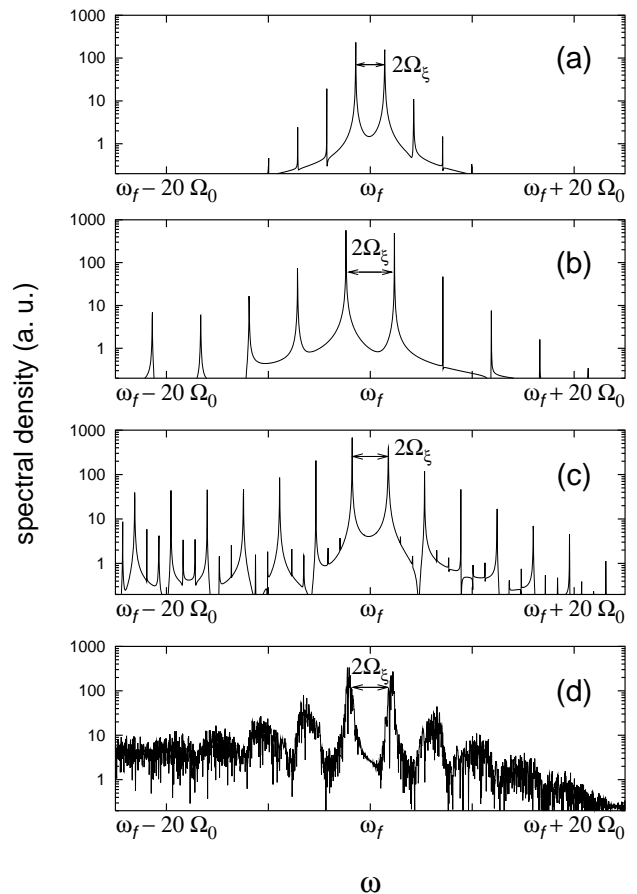


FIG. 5: Fluorescence spectra for trapped atoms in different regimes of oscillations: at $\delta = 24$: (a) period-1 limit cycle with $n = 3000$ photons, (b) period-1 limit cycle with $n = 10000$, (c) period-3 limit cycle with $n = 14846$, and (d) chaotic strange attractor with $n = 24000$. The frequency ω is shown in units of Ω_0 .

In order to check the conclusions mentioned above we integrate numerically Eq. (6) and compute the Fourier spectra of the quantity $(u - v) \cos \omega_f t - (u + v) \sin \omega_f t$ in different regimes of oscillations. In Fig. 5 spectra for different limit cycles for the same parameters as in Fig. 3 are shown. Fig. 5a demonstrate the spectrum of the quasi-harmonic period-1 limit cycle at $n = 3000$. In Fig. 5b a more complicated spectrum of the period-1 limit cycle at $n = 10000$ is shown. Fig. 5c demonstrate the spectrum of the period-3 limit cycle ($n = 14846$), and Fig. 5d is a spectrum of the chaotic strange attractor ($n = 24000$). A common feature of all the spectra is absence of odd harmonics $\omega_f \pm 2j \Omega_\xi / m$ ($j = 0, 1, 2, \dots$). For quasi-harmonic period-1 limit cycles, it can be shown analytically

in the framework of the approach described in Sec. IVB, that odd harmonics are really absent in the oscillations of the dipole-moment variables.

All the spectra refer to a single atom. A multiatom spectrum should be broadened because of a velocity distribution. However, the effect of velocity grouping, discussed in Sec. IIIB, should help to resolve the sidebands of the light emitted by an ensemble of atoms with limit cycles of low periods.

V. BIFURCATIONS

A. Synchronization map

Our nonlinear dissipative dynamical system demonstrates a rich variety of dynamical long-term regimes including periodic, quasiperiodic, and chaotic strange attractors. To illustrate this complexity we plot in Fig. 6 a synchronization map in comparatively small ranges of the detuning and the number of photons with fixed values of the other control parameters, $\alpha = 0.01$, $\gamma_a = 0.3$, and the same initial conditions. White color corresponds to period-1 limit cycles, nuances of grey color — to limit cycles of higher periods, and black color — to deterministic chaos. As the number of photons increases, higher harmonics in the spectrum become more and more prominent, and the approximated solutions (14) – (18) for period-1 limit cycles are no more valid. It is seen from the map that the limit cycles with higher periods appear practically for random values of the control parameters but inside prominent parallel bands separated by zones with period-1 limit cycles, exclusively. The border of chaos in Fig. 6 is jagged, and there exist nearby small “islands” of chaotic motion submerged into the “sea” of period-1 limit cycle motion.

The case of chaos we identify computing the maximal Lyapunov exponent λ which characterizes a mean velocity of diverging of initially closed trajectories in the phase space. The dependence of λ on the parameters δ and n is shown in Fig. 7 where color modulates values of λ . If $\lambda > 0$ the atomic oscillations are chaotic in a sense of sensitive dependence on initial conditions. A prominent asymmetry with respect to sign of the detuning δ is explained by different character of the force acting on atoms when $\delta > 0$ and $\delta < 0$ (see Sec. IIIB).

B. Bifurcation diagram

A general approach in studying the complexity of nonlinear dynamical systems involves investigating qualitative changes in their dynamics as system’s control parameters are varied. Sudden changes in the dynamics, known as bifurcations, occur when one of the control parameter crosses a critical value. The best way to visualize it is to compute so-called bifurcation diagrams. The bifurcation diagram in Fig. 8 shows dependence of negative values of

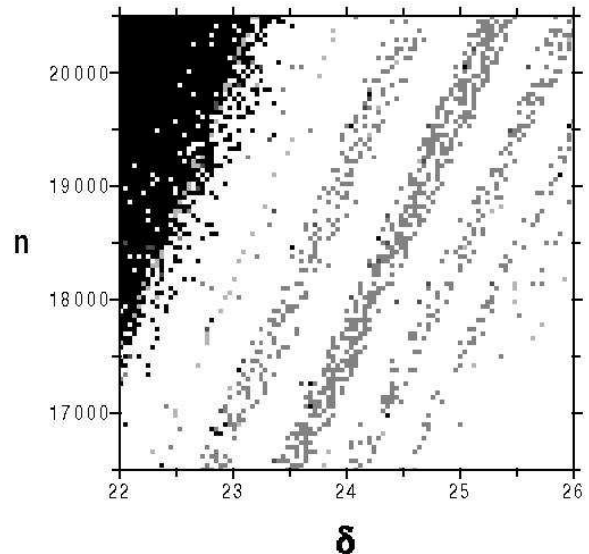


FIG. 6: Synchronization map in the plane of the average numbers of photons n and the detuning δ (in units of Ω_0): \square period 1 limit cycle, \square period 2 limit cycle, \square period 3 limit cycle, \square limit cycles with periods from 4 to 12, and \blacksquare chaos.

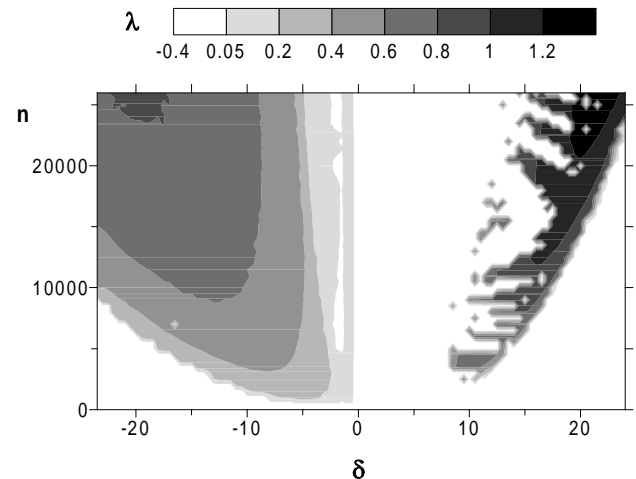


FIG. 7: Dependence of the maximal Lyapunov exponent λ on the average number of photons n and the detuning δ (λ and δ are shown in units of Ω_0).

the v -component of the atomic dipole of trapped atoms at the moments of time when $u = 0$ on the average number of photons n at fixed initial conditions and $\delta = 24$.

A general view in Fig. 8a demonstrates a complicated scenario of bifurcations on the road to chaos. In the range $n \lesssim 12000$, there exists a single stable limit cycle with period 1. At $12000 \lesssim n \lesssim 14000$, this cycle begins to multiply, i.e. there coexist in the phase space a few dif-

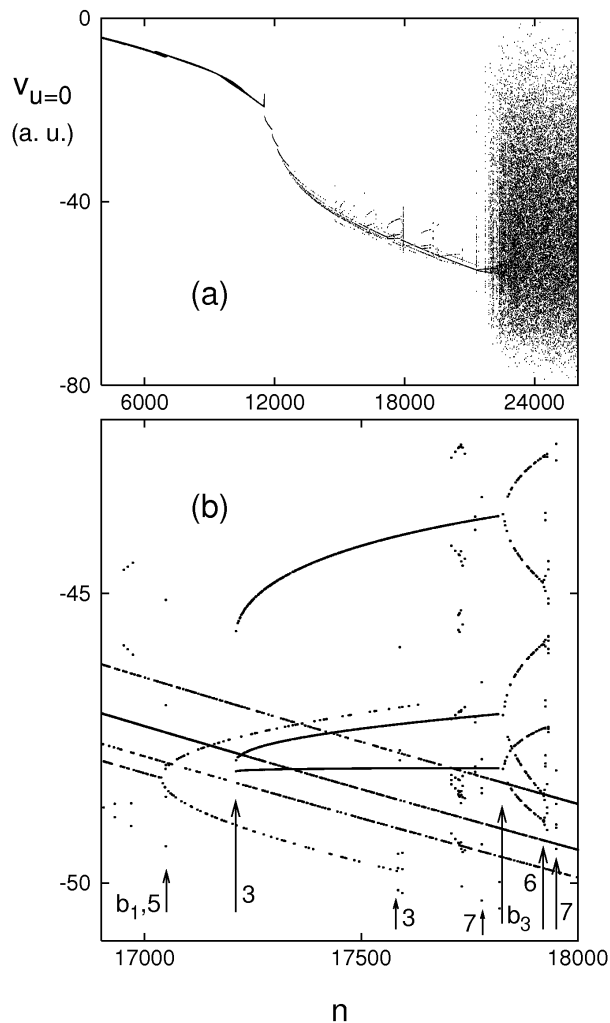


FIG. 8: Attractor bifurcation diagrams at $\delta = 24$: (a) a general view and (b) a cascade of bifurcations. Arrows $b_{1,3}$ indicate doubling of period-1 and period-3 limit cycles, respectively; 3, 5, and 7 — period-3, 5, and 7 limit cycles, respectively; 6 — period doubling bifurcation $3 \rightarrow 6$.

ferent period-1 limit cycles. Starting with a given initial state, an atom after a transition time reaches, of course, a definite period-1 limit cycle, but small changes in initial state may lead to another period-1 limit cycle. In other words, we know that in this range of n a period-1 limit cycle is settled after a transition time, but one cannot predict practically which one is reached. In the range $14000 \lesssim n \lesssim 21000$, a few cascades of bifurcations occur where limit cycles of higher periods appear.

A more detailed view in Fig. 8b helps to see a fine structure of one of the bifurcation cascades. We see that at $n \lesssim 17050$ practically all the points belong to four parallel lines. At a given value of n , only one value of v exists, but under small changes in n values of v jump randomly between the four lines. There really coexist

in the phase space four different limit cycles of period 1 with their own basins of attraction. A pitchfork b_1 at $n \simeq 17050$ means not a period doubling bifurcation but birth of two new limit cycles with period 1 from the old one. With n increasing further, real bifurcations with period m occur. We indicate them in Fig. 8b by the respective numbers. A prominent bifurcation of period 3 occurs at $n \simeq 17200$ when a period-3 limit cycle appears suddenly. Cycles of period 5 and 7 are also identified. Famous period doubling bifurcations are rather rare. One of them, corresponding to appearance a period-6 instead of a period-3 limit cycle, is indicated in Fig. 8b as “6”. In all the range, $16900 \lesssim n \lesssim 18000$, there coexist, at least, three period-1 limit cycles.

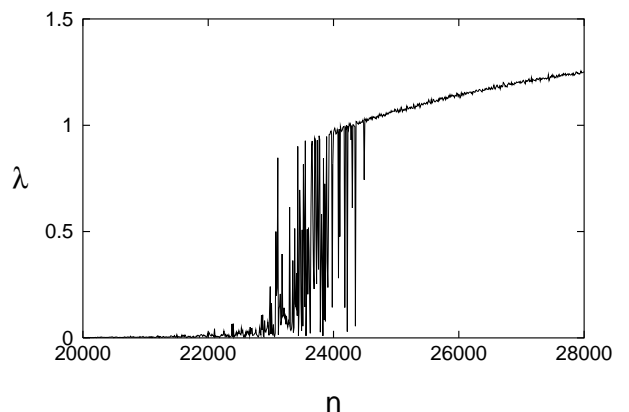


FIG. 9: Maximal Lyapunov exponent λ (in units of Ω_0) as a function of the average number of photons n at $\delta = 24$.

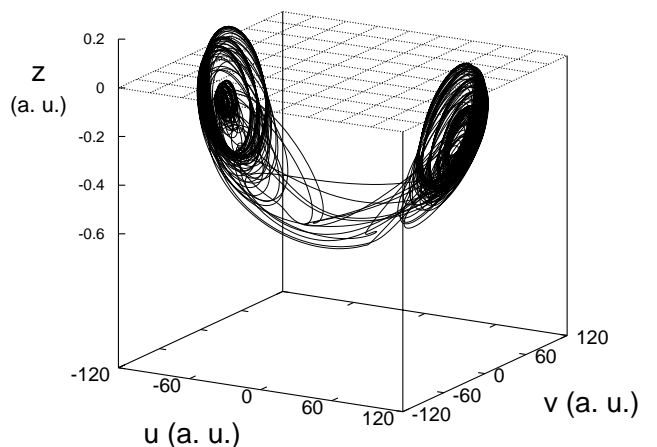


FIG. 10: Strange chaotic attractor in the Bloch sphere at $\delta = 24$ and $n = 24000$.

It is seen from Fig. 8a that, beginning with $n \approx 22000$, a complicated intermittent motion takes place. To con-

firm it, we compute in detail the dependence of the maximal Lyapunov exponent λ on the average number of photons n at $\delta = 24$. The plot in Fig. 9 demonstrates an intermittent road to a “stable” chaotic mode that is nothing more than a strange chaotic attractor. Its view in the Bloch space is shown in Fig. 10 with the parameter values $\delta = 24$ and $n = 24000$. Projections of this attractor on the planes (v, u) and (ξ, z) are shown in Fig. 3c. Its chaoticity is confirmed by computing the maximal Lyapunov exponent to be $\lambda \approx 1$, and its strangeness — by computing the Hausdorff dimension $d_F \approx 2.7$.

C. Influence of noise

The cascade of bifurcations in Fig. 8b is very complicated and its detailed analysis in the whole parameter space is practically impossible. We cannot expect, of course, that all the fine details of this cascade are relevant for real atoms in a standing wave. In order to know which limit cycles and bifurcations are expected to survive under an inevitable noise in real experiments, we incorporate a stochastic force into the right side of the second equation in the set (6) and compute again the bifurcation diagram shown in Fig. 8b at different levels of noise. Noise destroys the fine structure but the prominent period-1 and period-3 limit cycles with their characteristic properties do not disappear. In Fig. 11 we demonstrate the bifurcation diagram in the range $16900 \lesssim n \lesssim 18000$ under a weak broadband noise. Estimating the frequency of nonlinear oscillations of trapped atoms to be in the range $\omega_\xi \simeq 0.3 - 2$, we model the broadband noise by a linear combination of 100 harmonic functions with random phases and equidistantly distributed frequencies in the range from 0.05 to 5.

VI. FRACTAL RANDOM WALKING OF ATOMS

In Sec. III we have considered mechanical effects in regular atomic motion: acceleration, deceleration, velocity grouping, and trapping of atoms, all of which were characterized by negative or zero values of the maximal Lyapunov exponent λ . The Lyapunov map in Fig. 7 demonstrates that there exist wide ranges of the control parameters, n and δ , where atomic motion is expected to be exponentially sensitive to small changes in initial conditions. In the chaotic regime there also exist oscillations in wells of the optical potential and ballistic flights with an average velocity p_s . However, instead of stable limit cycles, there appear chaotic attractors (see Figs. 3c and 10), and the instant atomic velocity in the ballistic mode oscillates around p_s in an irregular way. In Fig. 12a we plot an example of a chaoticized velocity grouping (at $\delta = -24$, $n = 24000$, and $p_0 = 8$) that should be compared with the velocity grouping in regular regime in Fig. 2a. In difference from the regular velocity

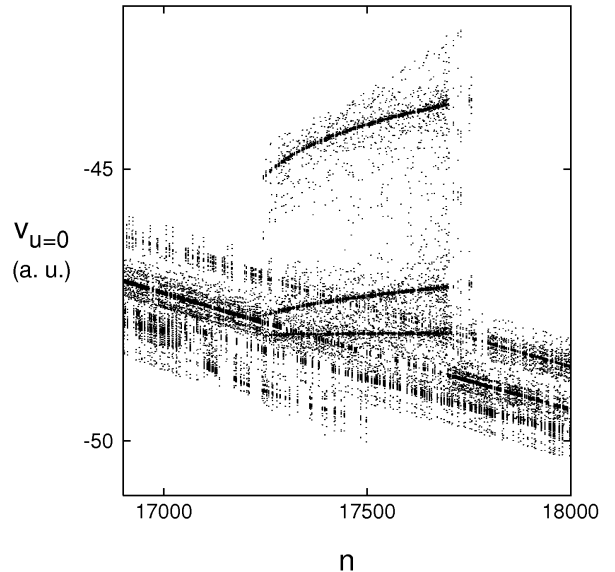


FIG. 11: Attractor bifurcation diagram at a weak noise. The other parameters and initial conditions are the same as in Fig. 8.

grouping, the momentum p_s , averaged over time of flying between two successive nodes of the standing wave, is not constant but oscillates slightly in an irregular way. With sufficiently large p_s it does not matter, in principle, but in some ranges of the control parameters a cardinal new type of motion takes place, when atomic motion is neither ballistic nor oscillating in wells but resembles strongly a random walking. In this regime an initially trapped atom oscillates in a well for a while, then it leaves the well for a ballistic flight and can be trapped in another well, etc. Random walking appears when there exist such zeroes of the friction force F where the grouping momentum p_s is close to the critical momentum p_{cr} (see Sec. IIIB). In the chaotic regime ($\lambda > 0$), p_s varies in an irregular way being either greater or smaller than p_{cr} . As an example, we demonstrate in Fig. 12b and c a random walking (at $\delta = -3$, $n = 24000$, and $p_0 = 50$) with a rather small grouping momentum $p_s \approx 30$.

Interesting properties of randomly walking atoms will be demonstrated with the following numerical experiment, a scheme of which is shown in Fig. 13. Atoms, one by one, are placed at the point $\xi = 0$ with the same initial momentum $p_0 = 50$ along the cavity axis. We compute the time T the atoms need to reach one of the detectors varying one of the control parameters, the average number of photons, n , or the detuning δ , and with the other parameters and initial conditions to be the same. To reduce numerical efforts, we restrict ourselves by 1D-geometry. The analogous numerical experiments for Hamiltonian atomic motion in a high-Q cavity have been done in Ref. [7] for a classical radiation field and in

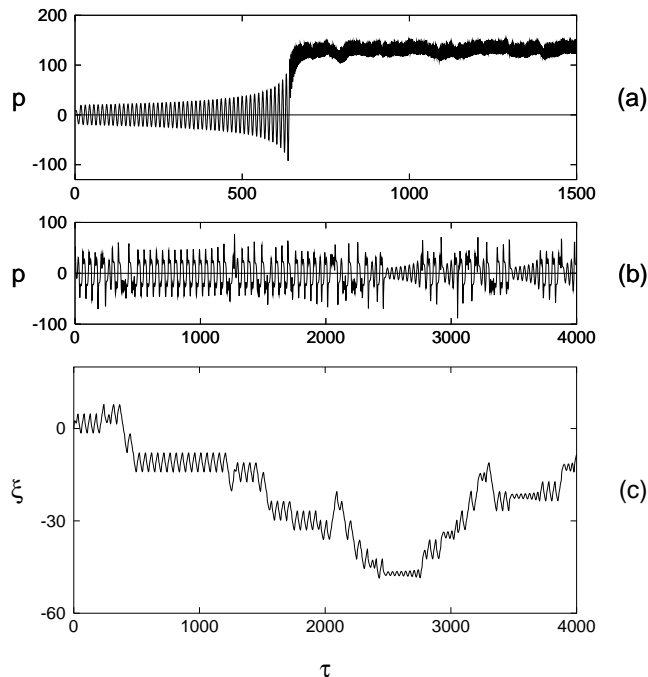


FIG. 12: Chaotic atomic motion: (a) chaotic velocity grouping at $\delta = -24$, (b) and (c) random walking at $\delta = -3$. Atomic position in units k_f^{-1} and momentum p in units $\hbar k_f$ as functions of time. Here $n = 24000$.

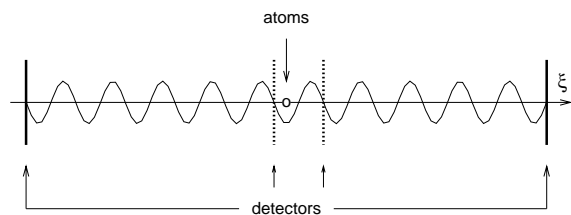


FIG. 13: Schematic diagram showing scattering of atoms at the standing wave when the space between detectors is equal to two (dashed lines) and twenty one wavelengths (bold lines).

Refs. [13, 18] for a quantized field in the Fock and coherent states of light. Self-similar hierarchical structures in the dependence $T(p_0)$ have been found in these papers. It seems to be more practical to compute the exit-time function in dependence on one of the parameters (n or δ) that is more easy to control than the initial atomic momentum.

The exit-time function $T(n)$ has been computed at $\delta = -3$ with two detectors placed at the distance of two lengths of the standing wave (dashed lines in Fig. 13 indicate places of the detectors in this case). Fig. 14 demonstrates an intermittency of smooth intervals and complicated structures that cannot be resolved in prin-

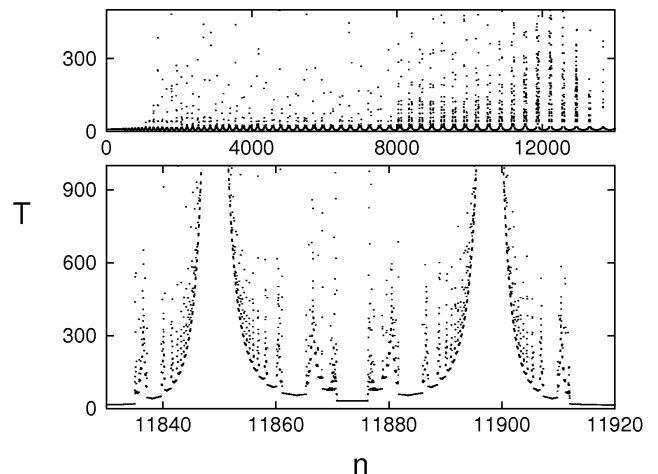


FIG. 14: Dependence of the exit time T (in units Ω_0^{-1}) on the number of photons n with different resolutions at $\delta = -3$ and $\gamma_a = 0.3$.

ciple no matter how large the magnification factor. The lower fragment of Fig. 14 is a zoom of the respective interval of the upper fragment. We see that even such a small zone of the atom-field interaction is enough to generate a complicated self-similar structure.

In order to prove that fractality is a robust property of randomly walking atoms, we compute the exit times T in dependence on the detuning δ with the space between detectors equal to 21 wavelengths. The result is shown in Fig. 15a at $n = 11880$ photons. Comparing it with the same function $T(\delta)$, but computed with two wavelengths, we see that the structure in Fig. 15b is more ordered demonstrating under zooming an intermittency of smooth and irregular parts with singularities.

The exit time T , corresponding to both the smooth and unresolved intervals, increases in average with increasing the magnification factor. There are also exist atoms never reaching the detectors in spite of the fact that they have no obvious energy restrictions to leave the small space between two detectors. There is an infinite number of unstable periodic orbits and chaotic orbits. The measure of such orbits is, of course, zero, and they cannot be exactly detected even in numerical experiments. However, such a sensitive dependence of the measured characteristic on the detuning should manifest itself in wild oscillations of the exit times in an arbitrary small neighbourhood of such values of δ where the scattering function $T(\delta)$ is singular, and the range of variation of T should not decrease to zero as the size of such a singular neighbourhood is reduced. The scattering function is singular on a Cantor set of values of the control parameter. It means that a relatively small uncertainty in the control parameters (or in initial values of dynamical variables) can often make prediction of the exit time practically

impossible. The fractal structure has been observed only with randomly walking atoms, i.e. at negative detunings. We have found complicated structures in the scattering function at $\delta > 0$, however under a magnification they appear to be smooth and without singularities.

To clarify the role of dissipation in forming fractal structures in the numerical scattering experiments, we plot in Fig. 16a the same dependence $T(\delta)$ but without dissipation, i.e. $\gamma_a = 0$. The fractal in Fig. 16a is a Hamiltonian one, and it possesses a beautiful self-similar structure with intermittent smooth and singular zones. Comparing Figs. 16a with $\gamma_a = 0$ and 15b with $\gamma_a = 0.3$, we see that the main part of this structure disappears under influence of dissipation. Instead of singularities, one can see smooth intervals in Fig. 15b. In order to demonstrate how it occurs, we plot in Fig. 16b the function $T(\delta)$ under the same conditions but with a reduced dissipation, $\gamma_a = 0.2$. In places of unresolved structures in Fig. 16a, we see some structures that, however, are resolved under a magnification into smooth intervals. We may conclude that spontaneous relaxation changes the fractal structure of the Hamiltonian scattering function. It smoothes second-order self-similar structures of the Hamiltonian fractal [7], but their border singular points become fractal-like dissipative structures.

VII. CONCLUSION

We have performed a theoretical and numerical study of the phenomenon of synchronization between internal and external degrees of freedom of atoms in a standing laser wave and of related topics. The character of the center-of-mass atomic motion can be understood with the help of the dependence of the friction force on the average momentum $F(|\bar{p}|)$. Zeroes of this function are either attractors or repellers. As a result, atoms tend to be grouped around respective values in the velocity space, the effect known as velocity grouping.

Synchronization is a common rhythm of co-existence of mechanical oscillations of atomic center-of-mass motion and internal Rabi oscillations that manifests itself in the phase space as limit cycles with different periods and riddled basins of attraction. We have derived a set of coupled equations for external and internal atomic vari-

ables and obtained approximated analytical solutions for period-1 limit cycles as for atoms, trapped in wells of the optical potential, as for ballistic atoms. The feasible way to detect synchronization in real experiments is to measure spectra of atomic fluorescence which for a period- m limit cycle should contain sideband frequencies, $\omega_f \pm jk_f v_s/m$ (ballistic atoms), or $\omega_f \pm j\Omega_\xi/m$ (trapped atoms). Due to the velocity grouping, limit cycles can be detected in spectra of light emitted by an ensemble of atoms with an initial velocity distribution.

Increasing the number of photons in the standing wave n , we have found cascades of bifurcations with higher periods to appear which eventually settle in a “stable” chaotic strange attractor with a positive value of the maximal Lyapunov exponent λ and a fractional Hausdorff dimension. A broadband noise, added to the equations of motion, destroys a fine structure of the cascades, but the prominent period-1 and period-3 limit cycles survive under a weak noise.

Computing the Lyapunov map, we have found wide ranges of the control parameters, n and the detuning δ , where $\lambda > 0$, and the atomic motion is expected to be chaotic either in the form of strange attractors in the wells or as flights with irregular oscillations of the velocity. Moreover, there exists a regime where the atomic motion is neither one of them but resembles strongly a random deterministic walking with erratically jumping atoms. The random walking is fractal in the sense that a scattering function is very sensitive to small changes in the control parameters or initial conditions and has a self-similar structure with singularities on a Cantor set of values of one of the control parameters. We have demonstrated it by computing a time of exit of atoms from a given space of the standing wave in dependence on n or δ .

VIII. ACKNOWLEDGMENTS

The work was financially supported by the Program of the Prezidium of the Russian Academy of Sciences, by the Russian Foundation for Basic Research (project 02-02-17796) and by the Far-Eastern Division of the Russian Academy of Sciences.

-
- [1] V.G. Minogin, V.S. Letokhov, *Laser Light Pressure on Atoms*, Gordon and Breach, New York (1987).
 - [2] A.P. Kazantsev, G.I. Surdutovich, and V.P. Yakovlev, *Mechanical Action of Light on Atoms*, World Scientific, Singapore (1990).
 - [3] C. Cohen-Tannoudji, J. Dupont-Roc, and G. Grynberg, *Atom-Photon Interaction — Basic Processes and Applications* (Wiley, New York, 1992).
 - [4] S. Stenholm, *Rev. Mod. Phys.* **58**, 699 (1986).
 - [5] C.S. Adams, M. Siegel, and J. Mlynek, *Phys. Rep.* **240**, 143 (1994).
 - [6] A. Vaglica, *Phys. Rev. A* **58**, 3856 (2001).
 - [7] V.Yu. Argonov and S.V. Prants, *Zh. Eksp. Teor. Fiz.* **123**, 946 (2003) [*JETP* **96**, 832 (2003)].
 - [8] M.Yu. Uleysky, L.E. Kon'kov, and S.V. Prants, *Comm. Nonlin. Sci. Numer. Simul.* **8**, 320 (2003).
 - [9] S.V. Prants and L.E. Kon'kov, *Pis'ma Zh. Éksp. Teor. Fiz.* **73**, 200 (2001) [*JETP Lett.* **73**, 180 (2001)].
 - [10] S. V. Prants and V. Yu. Sirotkin, *Phys. Rev. A* **64**, 033412 (2001).

- [11] S. V. Prants, M. Edelman, and G. M. Zaslavsky, Phys. Rev. E **66**, 046222 (2002).
- [12] S.V. Prants, Pis'ma Zh. Éksp. Teor. Fiz. **75**, 777 (2002) [JETP Letters **75**, 651 (2002)].
- [13] S.V. Prants and M.Yu. Uleysky, Phys. Lett. A **309**, 357 (2003).
- [14] A.P. Kazantsev, Zh. Eksp. Teor. Fiz. **66**, 784 (1974) [Sov. Phys. — JETP **39**, 784 (1974)].
- [15] Ch. Huygens, *Horologium Oscillatorium* (Apud F. Muguet, Parisiis, France, 1673) [English translation: *The Pendulum Clocks* (Iowa State University Press, Ames, 1986)].
- [16] A. Andronov and A. Witt, Zh. Prikl. Fiz. **7**(4), 3 (1930).
- [17] J. C. Sommerer, E. Ott, Nature **365**, 138 (1993).
- [18] S.V. Prants, in: *Chaotic Dynamics and Transport in Classical and Quantum Systems*, edited by G. Zaslavsky and M. Courbage (Kluwer Academic Publishers, Dordrecht, NATO ASI Series E, 2004).

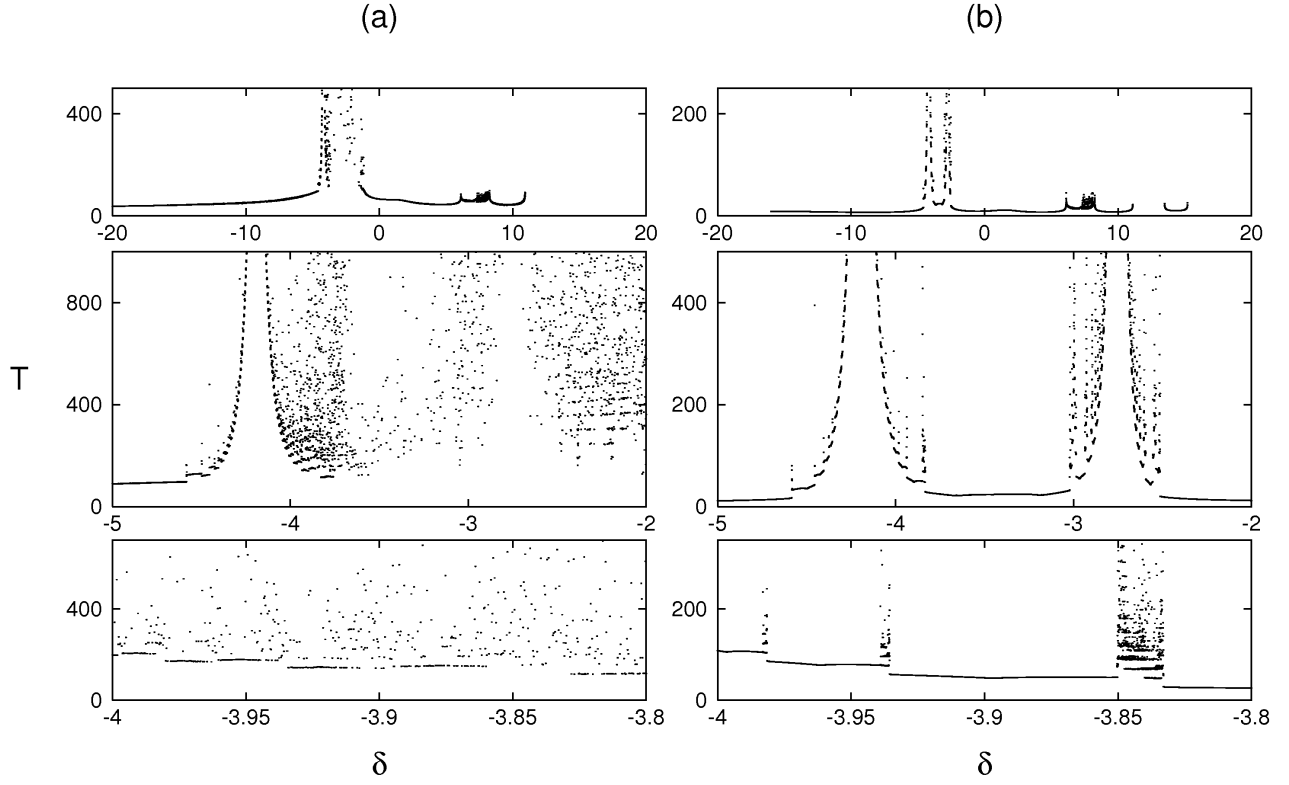


FIG. 15: Dependence of the exit time T (in units Ω_0^{-1}) on the detuning δ (in units of Ω_0) with different resolutions at $n = 11880$ and $\gamma_a = 0.3$: (a) the space between detectors is 21 wavelengths and (b) 2 wavelengths.

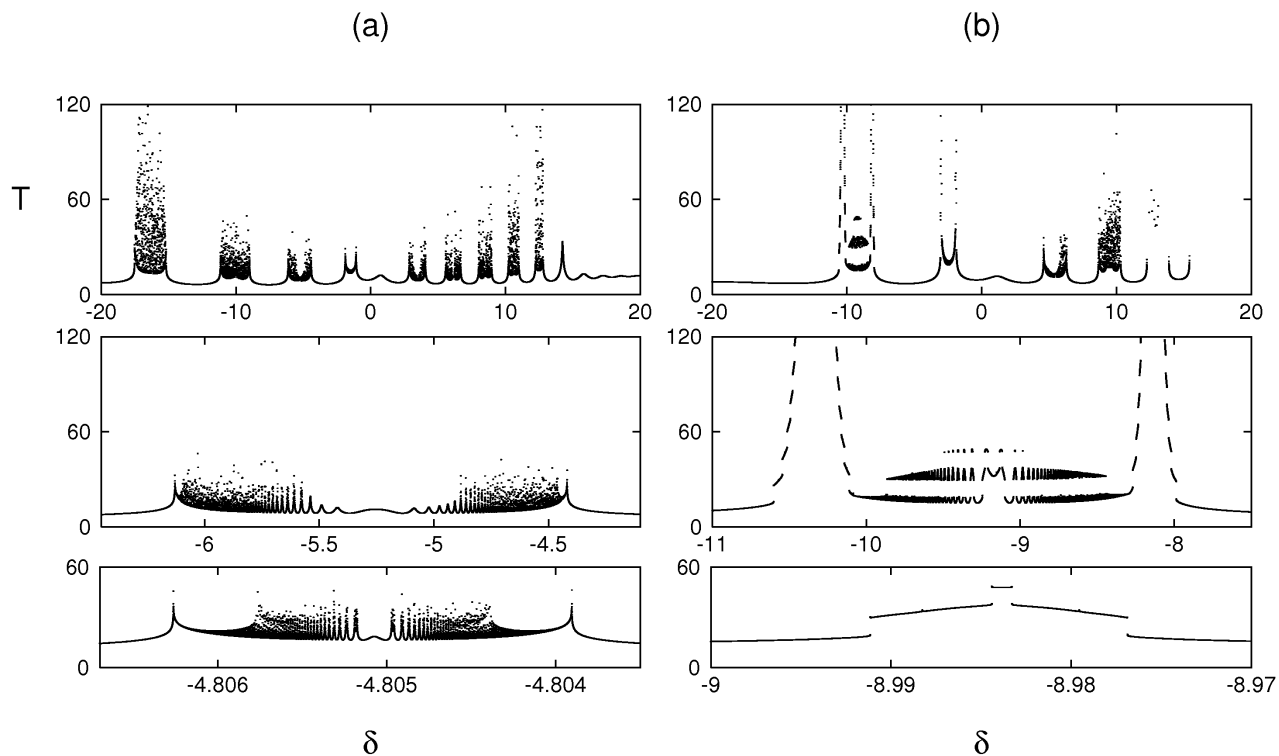


FIG. 16: Comparing Hamiltonian fractal with $\gamma_a = 0$ (a) and dissipative fractal with $\gamma_a = 0.2$ (b).